https://doi.org/10.1016/j.ultras.2015.10.026

Subarray Coherence Based Postfilter for Eigenspace Based Minimum Variance Beamformer in Ultrasound Plane-wave Imaging

Jinxin Zhao[1, 3], Yuanyuan Wang[1, 2], Jinhua Yu[1, 2], Wei Guo[1], Tianjie Li[3], and Yong-Ping Zheng[3]

1 Department of Electronic Engineering, Fudan University, Shanghai 200433, China

2 Key Laboratory of Medical Imaging Computing and Computer Assisted Intervention (MICCAI) of Shanghai, Shanghai 200433, China

3 Interdisciplinary Division of Biomedical Engineering，The Hong Kong Polytechnic University Hong Kong, HKSAR，China

Abstract—This paper introduces a new beamformer for ultrasound plane-wave imaging, which combines the eigenspace based minimum variance (ESBMV) beamformer with a subarray coherence based postfilter (SCBP). The ESBMV beamformer has been validated in improving the imaging quality due to its ability of noise reduction. However, the image contrast may still be low in the low SNR scenarios such as in plane-wave imaging, even with an overestimated noise removal. The overestimation of the noise in the eigen-analysis may also lead to dark-spot artifacts in the speckle, which limits the usage of the ESBMV. An SCBP scheme was proposed to improve the ESBMV performance in this study. As analyzed in this paper, the implementation of a traditional Wiener postfilter could be affected by the subarray technique. Accordingly, it was proposed to use the coherent and incoherent power on the subarray domain to compute a Wiener-like postfilter weight. Simulated and experimental data were used to evaluate the performance of the proposed approach. The results showed that the ESBMV-SCBP method achieved an enhanced imaging resolution and contrast compared with the ESBMV beamformer. In the simulation case, the contrast ratio (CR) and contrast-to-noise ratio (CNR) of an anechoic cyst were improved by 6% and 31% over the ESBMV. In the experimental case, the CR improvements for two anechoic cysts were 19% and 16% while the CNR improvements were 25% and 20%, respectively. These results demonstrated the effectiveness of the ESBMV-SCBP scheme. The ESBMV-SCBP also showed

advantages over the ESBMV-Wiener beamformer in preserving a more natural speckle. With a relatively small extra computational load, the proposed method has potential to enhance the imaging quality of ultrasound plane-wave imaging.

Keywords: Eigenspace based minimum variance beamformer, Coherence, plane-wave imaging, Subarray, Wiener postfilter

1. Introduction

Ultrasound plane-wave imaging has attracted increasing research interests in recent years. It is regarded as a proper method in achieving a high imaging frame rate [1] and is also beneficial to the development of some other kinds of ultrasonography [2, 3]. However, the high imaging frame rate is at the cost of a lower imaging quality due to the lack of focusing in the beam transmission. Plane-wave compounding [4, 5] could be a compromise for the imaging quality and frame rate, but it usually requires quite a number of plane waves to obtain a satisfactory compounding result, which decreases the frame rate to some extent.

Another method for enhancing the plane-wave imaging quality involves the application of adaptive beamformers. Unlike the traditional DAS method, which uses a fixed window for summation, adaptive beamformers compute a data-dependent weighting function to obtain a narrower mainlobe and lower sidelobes. It has been applied to ultrasound imaging and validated in enhancing the imaging quality by many researchers [6-12]. Besides the theoretical application of adaptive beamformers in ultrasound imaging, some recent studies have realized the adaptive beamforming in practical platforms for real-time imaging [13, 14].

Currently there are mainly two kinds of adaptive beamformers: the minimum variance (MV) based beamformers and the coherence factor (CF) based beamformers. The most representative beamformer of the former kind is the MV or also called as Capon beamformer, which was originally introduced by Capon in 1969 [15]. The aim of the MV beamformer is to minimize the output energy. Several techniques have been developed for its application in ultrasound imaging [9, 10, 16, 17]. Based on the MV

beamformer, the eigenspace based minimum variance (ESBMV) beamformer is then proposed for ultrasound imaging [7, 18, 19]. By projecting the MV weights onto the signal subspace, the ESBMV beamformer can remove a large part of the noise, which is helpful to enhance the image contrast. However, it is sometimes hard to divide the signal subspace and the noise subspace, which limits the effect on imaging enhancement [18, 19].

The second kind of adaptive beamformer is the CF-based beamformers [6, 11, 12, 20]. Unlike the MV-based adaptive beamformers, CF-based beamformer does not change the signal-to-noise ratio (SNR) of the beamformer output, but tries to decrease the mean square error (MSE). It attenuates the signal and noise part in the output to the same extent and is not a distortionless beamformer. The CF was originally defined as the ratio between the coherent power (CP) and the incoherent power (ICP). It can be viewed as a measurement of the focusing quality [12] and is suggested to be a correction for the array signal summation to suppress the noise and sidelobe. Li *et al.* [12] expanded the CF definition and proposed the generalized coherence factor (GCF) to be a better choice for practical application.

Some studies have focused on the combination of the CF with the MV-based beamformers. The MV-CF beamformer showed effectiveness in improving imaging resolution and contrast [6]. The high-resolution coherence factor (HRCF) was then proposed to be a better choice for the combination with the MV beamformer to achieve a higher resolution [21]. In another study, a theoretical framework was provided [20] to connect the CF with the Wiener postfilter. It was concluded that the CF could be seen as a factor, which amplifies the noise in the Wiener postfilter by M times (M is the element number of the array). A scaled Wiener postfilter was then suggested to make a compromise between the performance and robustness. In addition, a Wiener postfilter could be used to modify the performance for any kind of distortionless beamformer [19, 20]. Zeng *et al.* [19] described an ESBMV-Wiener beamformer and demonstrated its improvement in the imaging resolution, contrast and robustness over the ESBMV beamformer. Although the CF and Wiener postfilter performed well in sidelobe reduction, they also attenuated the signal power, which may cause artifacts and image degradation [19, 20]. This is true especially for the CF [20, 22, 23]. Besides, the output noise power in the Wiener postfilter is hard to

estimate. In [20], the white noise assumption was applied for the implementation of the Wiener postfilter, but it is usually not accurate. An SNR dependent coherence based method was proposed in [22] to overcome the shortcoming of the CF method. The coherence based postfilter is similar to the scaled Wiener postfilter in both the concept and the form. The advantage is that it only uses the coherent and incoherent energy and does not need to know the noise power in the output. The scaled factor is determined by a sigmoid function to adjust the postfilter between the Wiener-like postfilter and the CF factor. The method shows a significant image enhancement than the CF, but the parameters in the sigmoid function need to be carefully chosen according to the imaging object and the system SNR.

In this paper, we proposed a new beamformer by combining the ESBMV beamformer with a subarray coherence based postfilter. We first analyzed the effect of the spatial smoothing on the postfilter design, which has not attracted enough concern before. Inspired by the spatial-temporally smoothed coherence factor [23], we then attempted to use the coherence factor in the subarray to form a Wiener-like postfilter for the ESBMV beamformer. The postfilter would attenuate the noise part remained in the eigen-analysis output. As an overestimated noise subspace (namely a lower rank of signal subspace) may distort the speckle pattern [18], a combination of the SCBP with an underestimated noise subspace in the ESBMV beamformer is potential to improve the imaging quality with reduced damage to the speckle. Experiments were conducted on both the simulated and experimental data to evaluate the performance of the proposed beamformer. The results showed that the proposed method could achieve a better imaging contrast than the MV, ESBMV, and ESBMV-Wiener beamformers, while maintaining similar imaging resolution as the ESBMV-Wiener beamformer.

The rest part of this paper is organized as follows: The mathematical background of the MV-based and CF-based beamformers is given in Section 2. The proposed method is introduced in Section 3. Section 4 first describes the simulation and experimental study, and then shows the results by the proposed method and other beamformers. Discussion on the proposed method and the results is given in Section 5. Finally, a brief summary of the study is presented in Section 6.

2. Background

2.1 MV-based adaptive beamformers

We assume a linear transducer array with M elements. For each imaging point, the array signal after the time delay compensation can be expressed as

$$\mathbf{x}(n) = [x_1(n), x_2(n), ... x_M(n)]^{\mathrm{T}}, \tag{1}$$

where $(\cdot)^{\mathrm{T}}$ denotes the matrix transpose. While the DAS beamformer just averages the array data as the output, the MV beamformer uses an adaptive weighting vector $\mathbf{w}(n)$ for the signal summation, as follows:

$$z(n) = \mathbf{w}^{\mathrm{H}}(n)\mathbf{x}(n), \tag{2}$$

where $(\cdot)^{\mathrm{H}}$ denotes the conjugate transpose. The MV optimization problem can be expressed as

$$\min\ E[(z(n))^2] = \min\ \mathbf{w}^{\mathrm{H}}\mathbf{R}(n)\mathbf{w},\ \ \textit{subject to}\ \mathbf{w}^{\mathrm{H}}\mathbf{d} = 1. \tag{3}$$

Here $E[\cdot]$ is the expectation operator. The steering vector will become $\mathbf{d}$ = [1,1,…1] after the time delay compensation. $\mathbf{R}(n) = E[\mathbf{x}(n)\mathbf{x}^{\mathrm{H}}(n)]$ is the covariance matrix of the array data. The solution to (3) is calculated by

$$\mathbf{w}_{\mathrm{MV}} = \frac{\mathbf{R}^{-1}\mathbf{d}}{\mathbf{d}^{\mathrm{H}}\mathbf{R}^{-1}\mathbf{d}}. \tag{4}$$

There are several practical issues that should be considered. Firstly, the covariance matrix $\mathbf{R}$(n) is unknown and has to be estimated using the delayed array data as

$$\hat{\mathbf{R}}(n) = \mathbf{x}(n)\mathbf{x}^{\mathrm{H}}(n). \tag{5}$$

This estimation may be inaccurate. Moreover, the MV beamformer was originally developed with uncorrelated signal assumption [9, 15], while the array data are usually highly correlated in ultrasound imaging. Thus, the spatial smoothing technique [9, 10, 24] should be applied to ensure the covariance matrix estimation $\hat{\mathbf{R}}(n)$ nonsingular. It means dividing the original transducer array into overlapped subarrays of size L and averaging the covariance matrix over all the subarrays, as

$$\hat{\mathbf{R}}(n) = \frac{1}{M-L+1} \sum_{k=1}^{M-L+1} \mathbf{x}_k(n)\mathbf{x}_k^{\mathrm{H}}(n), \tag{6}$$

where $\mathbf{x}_k(n) = [x_k(n), x_{k+1}(n), ... x_{k+L-1}(n)]^{\mathrm{T}}$ denotes the kth subarray data. To enhance the robustness of the estimation, a small constant ε may also be used to add a noise onto $\hat{\mathbf{R}}(n)$, which means replacing it with $\hat{\mathbf{R}}(n) + \varepsilon \cdot \mathbf{I}$, where ε is a constant and $\mathbf{I}$ is the unitary matrix with the size of L. This is called the diagonal loading [9, 10]. The loading factor ε is usually set $\delta \cdot trace(\hat{\mathbf{R}})$ (δ is a small factor, usually less than 0.1). The final MV output is:

$$z_{\mathrm{MV}}(n) = \frac{1}{M-L+1} \sum_{k=1}^{M-L+1} \mathbf{w}_{\mathrm{MV}}^{\mathrm{H}}(n)\mathbf{x}_k(n). \tag{7}$$

For the ESBMV beamformer, the weight is computed based on the MV solution. The idea of the ESBMV beamformer is to use the eigen-analysis to remove the noise from the estimated covariance matrix. Therefore, $\hat{\mathbf{R}}(n)$ is firstly eigen decomposed as:

$$\hat{\mathbf{R}} = \mathbf{E}\,\mathbf{\Lambda}\,\mathbf{E}^{\mathrm{H}} = \sum_{i=1}^{L} \lambda_i \mathbf{v}_i \mathbf{v}_i^{\mathrm{H}}, \tag{8}$$

where $\mathbf{\Lambda} = diag[\lambda_1, \lambda_2, ... \lambda_L]$ denotes the eigenvalue matrix with all the eigenvalues in the descending order $\lambda_1 > \lambda_2 > ... > \lambda_L$. $\mathbf{v}_{\mathrm{i}}$ is the corresponding eigen vector to the eigenvalue λ_{i}. In the straightforward eigenvalue thresholding method [7], a threshold λ_{thre} is then used to divide the covariance matrix into the signal subspace and the noise subspace:

$$\mathbf{R} = \mathbf{E}\,\mathbf{\Lambda}\,\mathbf{E}^{\mathrm{H}} = \mathbf{E}_{\mathrm{s}}\mathbf{\Lambda}_{\mathrm{s}}\mathbf{E}_{\mathrm{s}}^{\mathrm{H}} + \mathbf{E}_{\mathrm{n}}\mathbf{\Lambda}_{\mathrm{n}}\mathbf{E}_{\mathrm{n}}^{\mathrm{H}} = \mathbf{R}_{\mathrm{s}} + \mathbf{R}_{\mathrm{n}}, \tag{9}$$

where $\mathbf{\Lambda}_{\mathrm{s}} = diag[\lambda_1, \lambda_2, ...\lambda_{\mathrm{thre}}]$ represents the signal part and $\mathbf{\Lambda}_n = diag[\lambda_{\mathrm{thre}+1}, \lambda_{\mathrm{thre}+2}, ...\lambda_L]$ represents the noise and interference part. Usually the λ_{thre} is set α times the smallest eigenvalue $\lambda_{\min}$ (α>1) or β times the largest eigenvalue $\lambda_{\max}$ (β<1) [19]. The ESBMV weights are then obtained by projecting the MV weights onto the signal subspace:

$$\mathbf{w}_{\mathrm{ESBMV}} = \mathbf{E}_{\mathrm{s}}\mathbf{E}_{\mathrm{s}}^{\mathrm{H}}\mathbf{w}_{\mathrm{MV}}. \tag{10}$$

2.2 CF-based methods and Wiener postfilter

As mentioned earlier, the CF is defined as the ratio between the CP and ICP [11, 12]:

$$\mathrm{CF} = \frac{\mathrm{CP}}{\mathrm{ICP}} = \frac{\left(\frac{1}{M}\sum_{i=1}^{M} x_i(n)\right)^2}{\frac{1}{M}\sum_{i=1}^{M}(x_i(n))^2}. \tag{11}$$

It is then suggested to be a correction for the DAS result to get a better noise reduction. For the MV beamformer, a similar concept is proposed [6, 21], which is called the HRCF:

$$\mathrm{HRCF} = \frac{(z_{mv})^2}{\frac{1}{M}\sum_{i=1}^{M}(x_i(n))^2}. \tag{12}$$

However, the CF or HRCF may cause artifacts in low SNR scenarios. In fact, the CF could be seen as a postfilter that amplifies the incoherent noise of a DAS-Wiener postfilter by M times [20]. This can be seen in the mathematical expression of the CF and Wiener postfilter H_{Wiener}:

$$\mathrm{CF} = \frac{\left(\frac{1}{M}\sum_{i=1}^{M} x_i(n)\right)^2}{\frac{1}{M}\left(\sum_{i=1}^{M} x_i(n)^2\right)} = \frac{\left(\frac{1}{M}\sum_{i=1}^{M} x_i(n)\right)^2}{\left(\frac{1}{M}\sum_{i=1}^{M} x_i(n)\right)^2 + \frac{1}{M}\sum_{i=1}^{M}\left(x_i(n) - \frac{1}{M}\sum_{i=1}^{M} x_i(n)\right)^2}, \tag{13}$$

$$H_{\mathrm{Wiener}} = \frac{|s|^2}{\mathbf{w}^{\mathbf{H}}\mathbf{R}\mathbf{w}} = \frac{|s|^2}{|s|^2 + \mathbf{w}^{\mathbf{H}}\mathbf{R}_p\mathbf{w}} \overset{\mathbf{w}=\mathbf{w}_{\mathrm{DAS}}}{=} \frac{\left(\frac{1}{M}\sum_{i=1}^{M} x_i(n)\right)^2}{\left(\frac{1}{M}\sum_{i=1}^{M} x_i(n)\right)^2 + \frac{1}{M^2}\sum_{i=1}^{M}\left(x_i(n) - \frac{1}{M}\sum_{i=1}^{M} x_i(n)\right)^2}. \tag{14}$$

Here the signal s is estimated using the beamformed output and $\mathbf{R}_p$ is estimated using the white noise assumption ($\mathbf{I}$ represents the unit matrix of size M):

$$\mathbf{R}_p = \frac{1}{M}\sum_{i=1}^{M}(x_i(n) - z(n))^2\,\mathbf{I}. \tag{15}$$

For any distortionless beamformer, a Wiener postfilter could be designed to modify the output. However, the noise matrix is not easy to obtain in the implementation. Nilsen *et al*. [20] suggested to use the white noise assumption but this may be inaccurate in ultrasound imaging. A similar concept is proposed [22, 25], which we call the coherence based (CB) postfilter in this paper. It is defined by

$$H_{\mathrm{CB}} = \frac{\mathrm{CP}}{\mathrm{CP} + \eta\,(\mathrm{ICP} - \mathrm{CP})} = \frac{\mathrm{CF}}{\mathrm{CF} + \eta\,(1 - \mathrm{CF})}\,. \tag{16}$$

In [22], the coefficient η is determined by using a sigmoid function of the SNR. If η is set to be 0, the H_{CB} is a constant 1; if η is set to be 1, the H_{CB} is equal to CF; if η is set to be *1/M*, then the CB postfilter is a Wiener-like postfilter in both the form and concept. Unlike in formula (14), the noise power here is obtained by directly subtracting the coherent power from the incoherent power. However, the parameters in the sigmoid function should be carefully chosen due to the imaging object and system SNR. It is better to have a user control as suggested in [22].

2.3 Effects of spatial smoothing on the Wiener postfilter

The theoretical framework about the relationship of the CF, Wiener postfilter and the CB postfilter is quite clear in Section 2.2. In this section, we focus on another issue in the MV-Wiener beamformer, which has not attracted enough concern. The spatial smoothing technique is originally designed for the implementation of the MV beamformer, but it may also affect the implementation of the Wiener postfilter. When no subarray is used, the beamformed output power will be $z^2=\mathbf{w}^{\mathbf{H}}\,\hat{\mathbf{R}}\,\mathbf{w}$. If z is used as the estimation of the signal s, and $\hat{\mathbf{R}}$ is used as the estimation of $\mathbf{R}$ in the Wiener postfilter, the H_{Wiener} will be constant to 1. However, when the spatial smoothing is used, the situation is different, due to the fact that $\hat{\mathbf{R}}$ is the averaged covariance matrix estimation of each subarray ($\sum_{k=1}^{M-L+1}\mathbf{x}_k(n)\mathbf{x}_k^{\mathrm{H}}(n)$), rather than the covariance matrix estimation of the averaged subarray ($(\sum_{k=1}^{M-L+1}\mathbf{x}_k(n))(\sum_{k=1}^{M-L+1}\mathbf{x}_k^{\mathrm{H}}(n))$). Accordingly, even when the noise matrix is unknown, the Wiener postfilter could still be implemented by

$$H_{\text{Wiener}} = \frac{|s|^2}{\mathbf{w}^{\mathbf{H}}\mathbf{R}\mathbf{w}} = \frac{|z|^2}{\mathbf{w}^{\mathbf{H}}\hat{\mathbf{R}}\mathbf{w}}. \tag{17}$$

This accords with the fact that the Wiener beamformer [20] can be obtained by combining a Wiener postfilter with a distortionless beamformer, for example the MV beamformer:

$$\begin{aligned}\mathbf{w}_{\text{Wiener}} &= |s|^2 \mathbf{R}^{-1}\mathbf{d} = |z|^2 \hat{\mathbf{R}}^{-1}\mathbf{d} = \frac{\hat{\mathbf{R}}^{-1}\mathbf{d}}{\mathbf{d}^{\text{H}}\hat{\mathbf{R}}^{-1}\mathbf{d}}|z|^2 \mathbf{d}^{\text{H}}\hat{\mathbf{R}}^{-1}\mathbf{d} \\ &= \frac{\hat{\mathbf{R}}^{-1}\mathbf{d}}{\mathbf{d}^{\text{H}}\hat{\mathbf{R}}^{-1}\mathbf{d}} \frac{|z|^2}{(\frac{\hat{\mathbf{R}}^{-1}\mathbf{d}}{\mathbf{d}^{\text{H}}\hat{\mathbf{R}}^{-1}\mathbf{d}})^{\text{H}}\hat{\mathbf{R}}\frac{\hat{\mathbf{R}}^{-1}\mathbf{d}}{\mathbf{d}^{\text{H}}\hat{\mathbf{R}}^{-1}\mathbf{d}}} = \mathbf{w}_{\text{MV}} H_{\text{Wiener}}\end{aligned}. \tag{18}$$

3. Methods

Due to the application of spatial smoothing, the adaptive weight aims at minimizing the averaged subarray coherent summation power instead of the original coherent summation power. Moreover, the above discussion reveals the possibility of implementing the Wiener postfilter even when the output noise matrix is unknown. The possibility results from the fact that the MV weight is designed practically on the subarray domain, while the Wiener postfilter design still focuses on the original array domain. Accordingly, we proposed to extend the CB postfilter concept to the subarray domain, which means using the subarray coherent power (SCP) and the subarray incoherent power (SICP) to design the Wiener-like SCBP. This could be expressed by

$$H_{\text{SCBP}} = \frac{\text{SCP}}{\text{SCP} + \eta\,(\text{SICP} - \text{SCP})}. \tag{19}$$

Here the SCP and the SICP are averaged over all the subarrays:

$$\text{SCP} = \frac{1}{M-L+1}\sum_{k=1}^{M-L+1}(\mathbf{w}^{\mathbf{H}}\mathbf{x}_k(n))^2 = \frac{1}{M-L+1}\sum_{k=1}^{M-L+1}\mathbf{w}^{\mathbf{H}}\mathbf{x}_k(n)\mathbf{x}_k^{\text{H}}(n)\mathbf{w} = \mathbf{w}^{\mathbf{H}}\hat{\mathbf{R}}\mathbf{w}, \tag{20}$$

$$\text{SICP} = \frac{1}{M-L+1}\sum_{k=1}^{M-L+1}\frac{1}{L}\mathbf{x}_k^{\text{H}}(n)\mathbf{x}_k(n). \tag{21}$$

As the length of the subarray is L instead of M, the parameter η is set to be $1/L$ to work like a Wiener

solution. Since the ESBMV beamformer ideally offers a more accurate estimation of the signal than the DAS and MV beamformers, the SCBP was then combined with the ESBMV beamformer to form an ESBMV-SCBP beamformer:

$$H_{\mathrm{ESBMV-SCBP}} = H_{\mathrm{SCBP}} \mathbf{w}_{\mathrm{ESBMV}} , \tag{22}$$

where the ESBMV weights $\mathbf{w}_{\mathrm{ESBMV}}$ is used in (19)-(21).

In the proposed ESBMV-SCBP method, the original array data are first realigned into overlapped subarrays, and then the adaptive ESBMV weights are computed based on the covariance matrix with the eigen-analysis. Finally, an SCBP for the subarray is designed to correct the ESBMV output. The spatial smoothing enhances the robustness of the MV-based weights computation, but also changes the objective energy function from the weighted coherent sum of all the element data (z_{MV}^2 or z_{ESBMV}^2) to the averaged coherent sum of subarray data (SCP). Therefore, we proposed to use the objective energy function $\mathbf{w}^{\mathbf{H}} \hat{\mathbf{R}} \mathbf{w}$ for the Wiener-like postfilter design. This objective energy function could also be viewed as the averaged CP of the subarrays, so the SICP is then used as the corresponding transformation of the ICP. The SCBP should be a superior choice than the CB postfilter to be combined with the adaptive weights as it is designed for the subarray aperture as same as the adaptive weighting function. Similar to a Wiener postfilter, it will further reduce the noise in the ESBMV, which may contribute to an image enhancement.

4. Experiments and results

Plane waves were used in both simulated and experimental studies to validate the performance of the proposed method. All the simulated data were generated by the Matlab simulation tool Field II [26]. All the phantom and human tissue data were acquired using the Verasonics ultrasound platform (V1, Verasonics, Redmond, WA).

In the simulation test, a 5-MHz, 128-element transducer array with a half-wavelength spaced pitch was used. The sampling rate was set to be 100 MHz to ensure accurate time delay compensation. A zero-mean Gaussian distributed noise with an SNR of 60 dB was added to each channel before the beamforming process. In the experimental study, a 6.944-MHz, 128-elements transducer array with a

pitch of 0.3mm (L11-4v, Verasonics, Redmond, WA) was adopted. The sampling rate was 27.776 MHz corresponding to a sample number of four in each transmitting wavelength. In all the cases, the excitation pulse was a two-cycle sinusoidal at the center frequency with a fractional bandwidth of 60%. A subarray length of L=48 was used and the diagonal loading factor ε is set as 0.01 times of the signal power in all the studies. For the point targets, an eigenvalue threshold β=0.1 was used. For the cyst or tissue target, β is set to be 0.05 to avoid severe damage to the speckle pattern. The imaging results of the proposed ESBMV-SCBP will be shown together with those of the DAS, MV, ESBMV, and ESBMV-Wiener for comparison.

4.1 Simulated study: point phantom

Four pairs of point targets were simulated in a homogeneous medium. They were located at z=30mm, 35mm, 40mm, and 45mm, respectively. The distance between each point pair was set as 1 mm. Fig .1 shows the responses of different beamformers with a dynamic range of 60 dB.

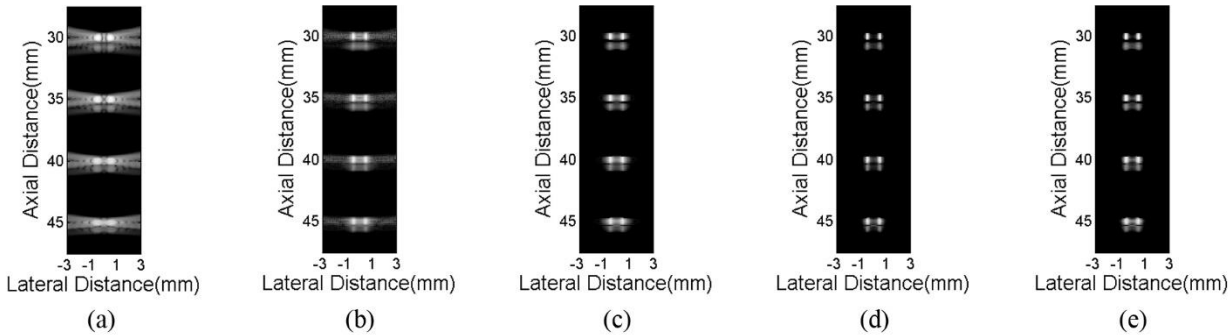

Fig. 1 Simulated point pair images of different beamformers: (a) DAS, (b) MV, (c) ESBMV, (d) ESBMV-Wiener, and (e) ESBMV-SCBP. All images are shown with a dynamic range of 60 dB.

A significantly narrower mainlobe in the MV image can be observed as shown in Fig. 1 (b) compared with the DAS result in Fig. 1 (a). In Fig. 1 (c), the ESBMV beamformer further reduced the sidelobe, but the mainlobe width remained almost the same as the MV result. It is still hard to separate the two points in the ESBMV image. The ESBMV-Wiener and the ESBMV-SCBP beamformers both

achieved a further improvement compared with the ESBMV. From Fig. 1 (d) and (e), it can be seen that they both succeeded in separating the two points for at least the point pair at the depth of z=30 mm.

The lateral variations of the ESBMV-based beamformers across each point pair are shown in Fig. 2. As the imaging depth increases, the point pair becomes harder to tell apart for all the beamformers due to a relatively smaller aperture size. In all the four subfigures, the ESBMV-Wiener maintains the best performance, and the mainlobe of the ESBMV-SCBP is only slightly wider. This indicates that both the ESBMV-based postfilters could further suppress the noise and sidelobe than the ESBMV beamformer, which contributes to a higher imaging resolution.

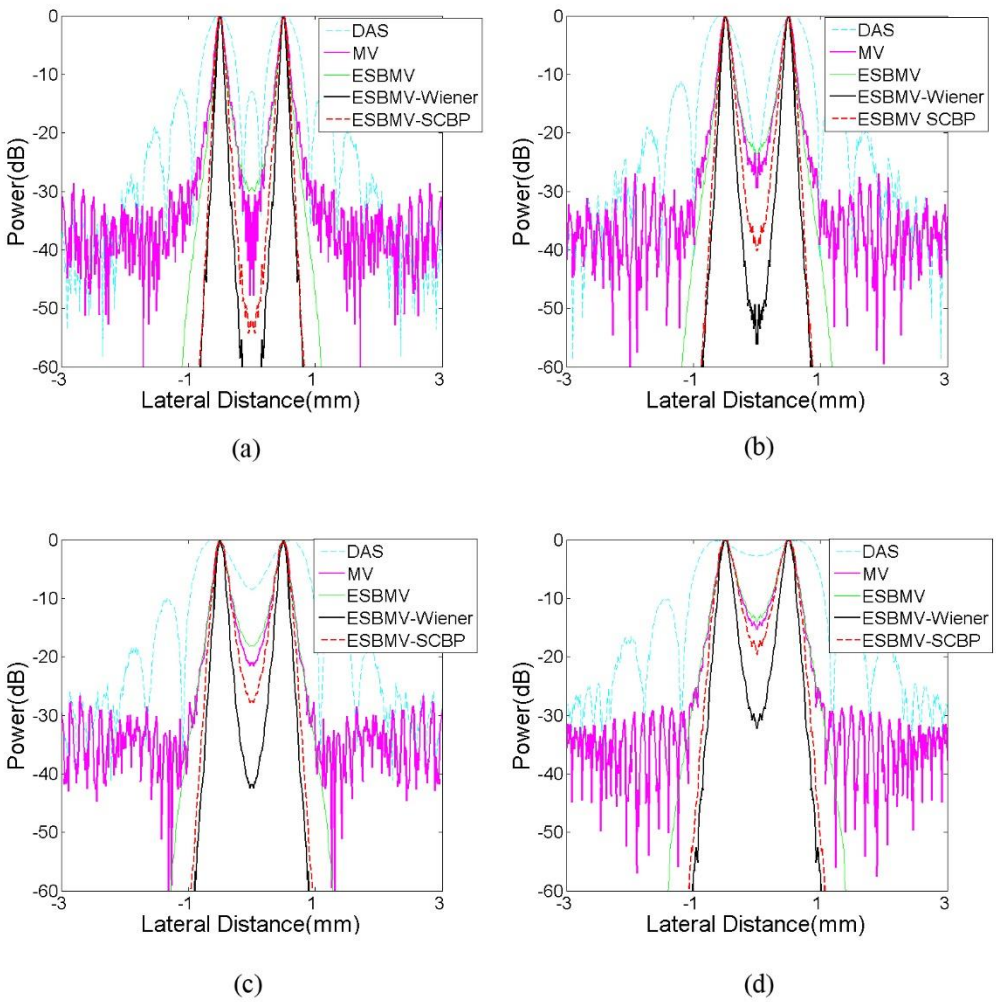

Fig. 2 Lateral variations of the point pairs at the depth of (a) z=30 mm, (b) z=35 mm, (c) z=40 mm, (d) z=45 mm.

4.2 Simulated study: cyst phantom

A 4-mm radius circular anechoic cyst was centered at (x, y, z) = (0, 0, 37 mm). Background speckles were generated by displacing randomly distributed scatterers with an intensity of 10 per unit of cubic wavelength λ^3. Fig. 3 presents the images of different beamformers with a dynamic range of 70 dB.

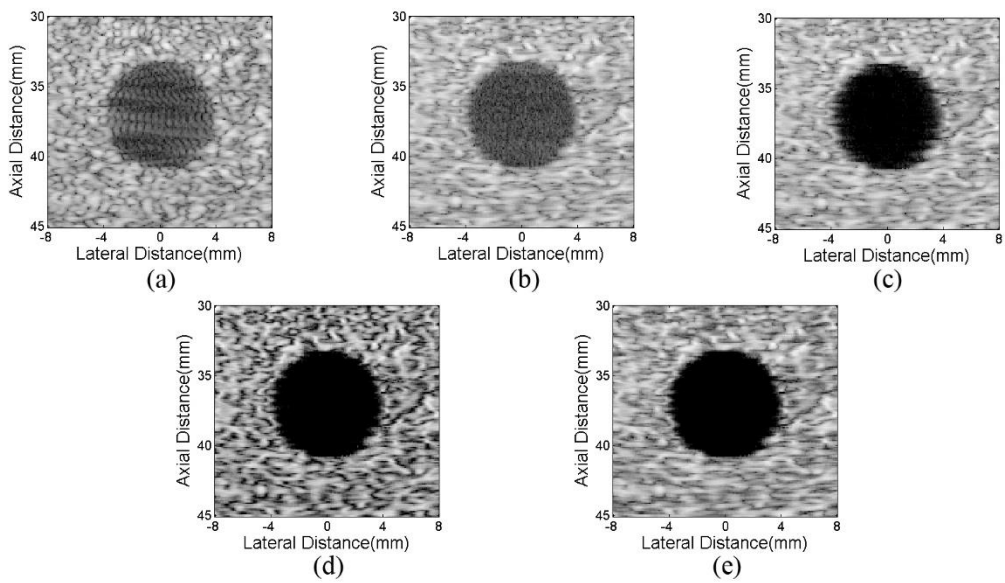

Fig. 3 Simulated cyst images of different beamformers: (a) DAS, (b) MV, (c) ESBMV, (d) ESBMV-Wiener, and (e) ESBMV-SCBP. All images are shown with a dynamic range of 70 dB.

It can be observed from Fig. 3 (a) and (b) that both the DAS and MV beamformers have a poor imaging contrast for the plane-wave imaging. When using the eigen-analysis, a large part of the noise was removed, which leads to a significant contrast enhancement and a much clearer cyst margin as displayed in Fig. 3 (c). The cyst edges in Fig. 3 (d) and (e) are even clearer, due to a further noise suppression inside the cyst region. The ESBMV-SCBP, by contrast, preserved a more natural speckle pattern than the ESBMV-Wiener, which darkens the black stripes in the speckle. The darkening of the speckle may lead to artifacts and image degradation.

We now assess the performances of different beamformers with the contrast ratio (CR) and the

contrast-to-noise ratio (CNR). The two ratios are defined by

$$\mathrm{CR} = \mu_b - \mu_c \,, \tag{23}$$

$$\mathrm{CNR} = \frac{|\mu_b - \mu_c|}{\sqrt{\sigma_b^2 + \sigma_c^2}} \,, \tag{24}$$

where μ_b and μ_c are the mean intensity of the cyst and speckle, and σ_b and σ_c are the intensity standard deviation of the cyst and speckle. The region of cyst is defined as the 4-mm radius circle centered at (x, y, z) = (0, 0, 37 mm). Table I gives the quantitative results. A contrast enhancement of 39% and 182% upon the DAS was achieved by the MV and ESBMV beamformers, respectively. The ESBMV-Wiener reduced the noise inside the cyst, but it also darkened the speckle brightness, which led to a 6% decline in CR and an 11% decline in CNR compared with the ESBMV beamformer. On the other hand, the ESBMV-SCBP beamformer could maintain a comparable speckle pattern while reducing the noise inside the cyst. It accomplished a 6% improvement in CR and a 31% improvement in CNR upon the ESBMV.

TABLE I

Contrast ratio (CR) and contrast-to-noise ratio (CNR) of simulated anechoic cyst for different beamformers

Beamformer	CR(dB)	CNR
DAS	15.76	1.76
MV	21.93	2.29
ESBMV	44.46	2.78
ESBMV-Wiener	41.82	2.48
ESBMV-SCBP	47.27	3.66

4.3 Experimental study: point phantom

A point target was located at (x, y, z) = (5, 0, 15) mm. Fig. 4 gives the results of different beamformers with a dynamic range of 60 dB.

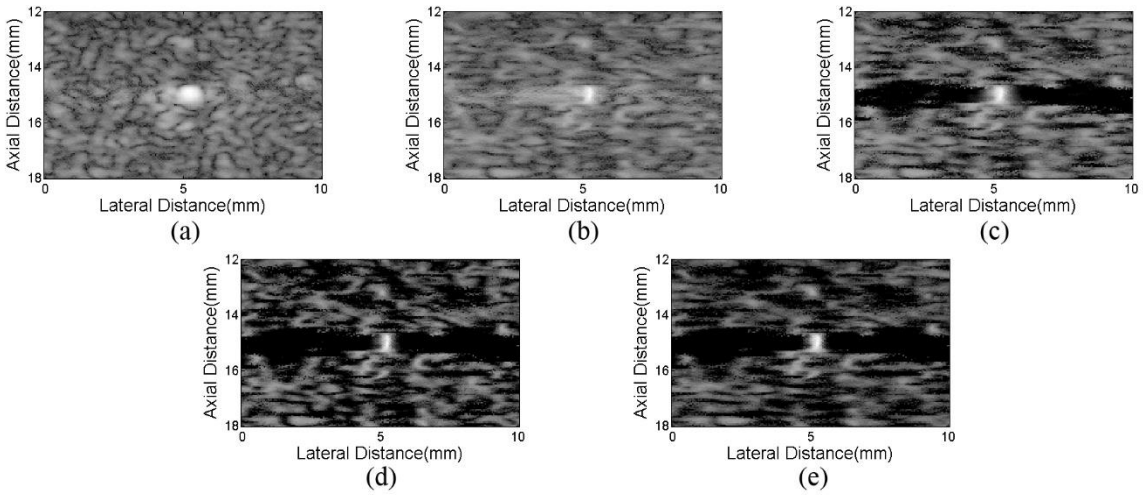

Fig. 4 Experimental point images of different beamformers: (a) DAS, (b) MV, (c) ESBMV, (d) ESBMV-Wiener, and (e) ESBMV-SCBP. All images are shown with a dynamic range of 60 dB.

Similar to the simulation case, the MV beamformer significantly narrowed the point mainlobe compared with the DAS beamformer. For the ESBMV-based beamformers, the noise reduction by the eigenspace projection generated a black artifact alongside the highlighted target as demonstrated in Fig. 4 (c)-(e)[18, 19], which is similar as in the CF method [20, 23]. The lateral variations across the point target is shown in Fig. 5. It can be seen that both the ESBMV-Wiener and the ESBMV-SCBP can achieve a better resolution than the ESBMV beamformer, while the ESBMV-Wiener seems to have a narrower mainlobe.

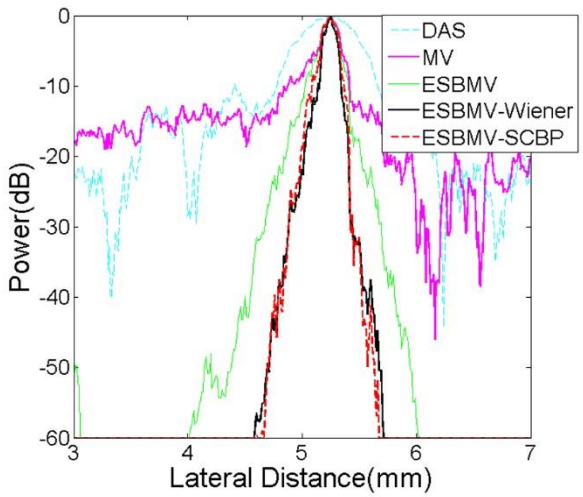

Fig. 5 Lateral variations of the point pairs at the depth of *z*=15 mm.

The full width at half maximum (FWHM) was used as the quantitative indicator of the mainlobe width. Table II shows the statistic result. The mainlobe width of the ESBMV-SCBP is a little wider than that of the ESBMV-Wiener, but is only 26%, 66% and 76% of that of the DAS, MV, and ESBMV beamformers, respectively.

TABLE II

Full width at half maximum (FWHM) for the beamformed responses at z=15 mm.

Beamformer	FWHM(mm)
DAS	0.73
MV	0.29
ESBMV	0.25
ESBMV-Wiener	0.17
ESBMV-SCBP	0.19

4.4 Experimental study: cyst-mimicking phantom

Two anechoic cysts were located at different depths. The beamformed results are shown in Fig. 6 with a dynamic range of 60 dB.

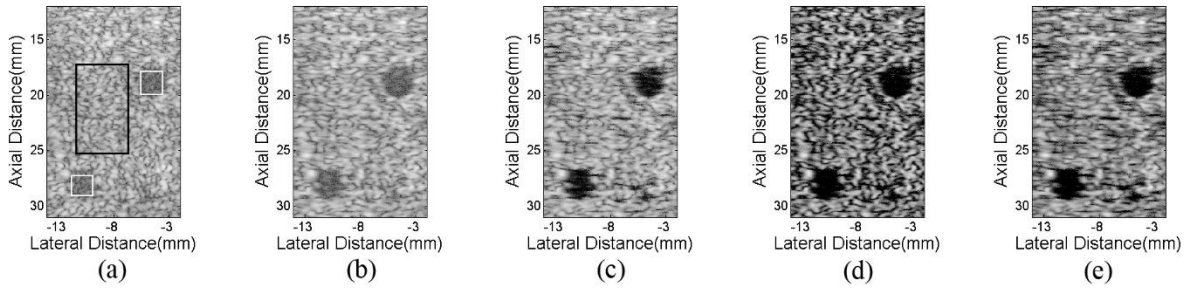

Fig. 6 Experimental cyst images of different beamformers: (a) DAS, (b) MV, (c) ESBMV, (d) ESBMV-Wiener, and (e) ESBMV-SCBP. All images are shown with a dynamic range of 60 dB.

The DAS and MV images suffer a low contrast (Fig. 6 (a) &(b)), and the contrast enhancement by eigenspace projection as shown in Fig. 6 (c) is limited due to the low SNR. A larger eigenvalue threshold can reduce the noise inside the cyst, but would cause severe damage to the speckle. In the ESBMV-Wiener or ESBMV-SCBP image, the noise inside the cyst was dramatically reduced and the cyst margin is much clearer. Similar to the simulation scenario, the ESBMV-Wiener darkened the black stripes in the speckle, while the background in the ESBMV-SCBP image is more similar to that of the ESBMV beamformer.

The CR and CNR were used to assess the performances of different beamformers. The region of interest (ROI) is illustrated in Fig. 6 (a) with two white boxes for the mimicked-cysts and a black box for the speckle. Table III gives the quantitative results. The ESBMV-SCBP beamformer achieved a CR improvement by 19% and 16% compared with the ESBMV beamformer for the two cysts, which is larger than the corresponding value of the ESBMV-Wiener (7% and 4%). Meanwhile, the ESBMV-Wiener caused a CNR decline, while the ESBMV-SCBP beamformer achieved a CNR improvement of 25% and 20% upon the ESBMV for the two cysts, respectively.

TABLE III

Contrast ratio (CR) and contrast-to-noise ratio (CNR) of the two phantom cysts for different beamformers.

Beamformer	CR(dB)	CNR
DAS	10.33/8.73	1.35/1.15
MV	13.27/12.60	1.72/1.66
ESBMV	31.07/32.71	2.64/3.04
ESBMV-Wiener	33.28/34.14	2.38/2.57
ESBMV-SCBP	37.03/37.94	3.30/3.66

4.5 Experimental study: clinical human tissue

Clinical data of a human carotid artery were acquired from the same Verasonics ultrasound system, and the results by the different beamformers are shown in Fig. 7 with a dynamic range of 70 dB.

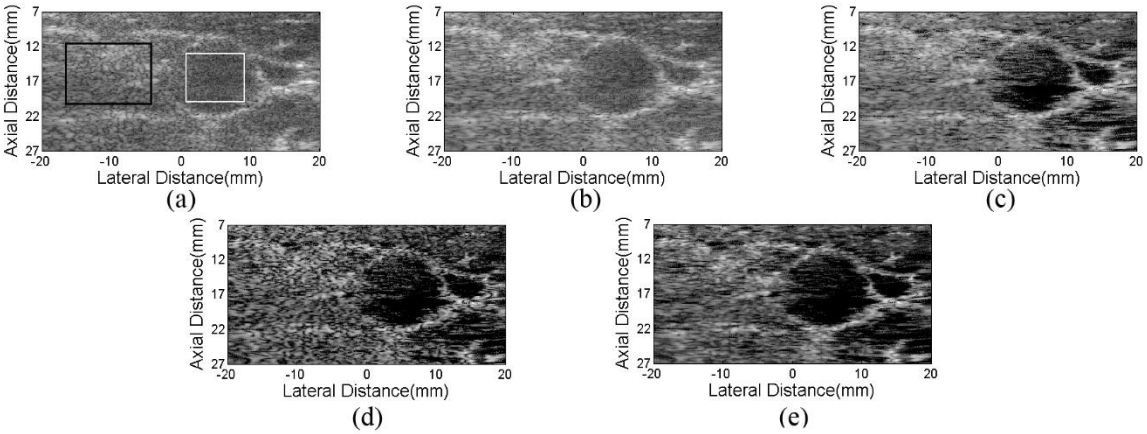

Fig. 7 Experimental carotid artery images of different beamformers: (a) DAS, (b) MV, (c) ESBMV, (d) ESBMV-Wiener, and (e) ESBMV-SCBP. All images are shown with a dynamic range of 70 dB.

In this situation, the target (carotid artery in the center) is surrounded by different objects with a large brightness variation range. As observed in Fig. 7, the ESBMV may cause some dark spot artifacts with a fixed eigenvalue threshold. Nevertheless, by comparison with the DAS or the MV images, the ESBMV beamformer still showed the ability to enhance the visualization of hyperechoic structures. The enhancement is more obvious in the ESBMV-SCBP image. Meanwhile, due to the darkening of black stripes, the speckle seems more splitted in the ESBMV-Wiener image, which is undesirable for the recognition of anatomical structures.

For the quantitative assessment, the ROI is illustrated in Fig. 7 (a) with a white box for the carotid artery and a black box for the background region. Table IV gives the quantitative values of the CR and CNR. Although the noise inside the artery was reduced, the CR and CNR of the ESBMV-Wiener image both decreased due to the darkening of the black stripes in speckle. Meanwhile, the ESBMV-SCBP beamformer achieved a 6% CR improvement and a 22% CNR improvement upon the ESBMV

beamformer.

TABLE IV
Contrast ratio (CR) and contrast-to-noise ratio (CNR) of carotid artery for different beamformers.

Beamformer	CR(dB)	CNR
DAS	7.58	0.85
MV	9.43	1.06
ESBMV	27.11	1.60
ESBMV-Wiener	26.39	1.41
ESBMV-SCBP	29.80	2.00

5. Discussions

Based on the above results, the proposed method showed its potential in enhancing the imaging resolution compared with the DAS, MV and ESBMV beamformers. The resolution enhancement is due to the noise reduction by the SCBP, which is similar to the Wiener postfilter. As shown in Fig. 2 and Fig. 5, in both the simulated and experimental tests, the ESBMV-SCBP exhibited a similar performance to the ESBMV-Wiener, with only a slightly wider mainlobe. For the anechoic cyst, the Wiener-SCBP beamformer showed its ability in reducing the off-axis interference from the surrounding speckle, which is also similar to the ESBMV-Wiener beamformer. However, due to the different schemes, they demonstrated very different performances on the surrounding speckle. In Fig. 3 and Fig. 6, it can be observed that the ESBMV-Wiener beamformer would darken the black stripes in the speckle, resulting a decline in the CNR and a degraded image. This would also lead to a splitted speckle pattern, which is not desirable for the visualization of anatomical structure as demonstrated in Fig. 7. Meanwhile for the proposed ESBMV-SCBP method, the speckle could be better preserved and thus a higher imaging contrast was obtained compared with the ESBMV-Wiener beamformer.

The coherence based Wiener-like postfilter is very similar to the Wiener postfilter in both the concepts and form. However, it assesses the array signals from the input domain rather than the output as in the Wiener postfilter. Using the coherent and incoherent power of the array, the noise model is not essential in computing the postfilter. As described in Section 2.3, the implementation of the Wiener postfilter is affected by the spatial smoothing, which is usually essential in the MV weights computation. Despite the decorrelation of the array signal, the spatial smoothing could also be viewed as a realignment

of the array signal into different subarray signals. This realignment decreases the array size from M to L, but the averaging over the M-L+1 subarrays increases the SNR of each subarray element signal. The covariance matrix is then estimated using the realigned subarrays. This means that the MV or ESBMV weight is designed for the realigned array. Accordingly, we proposed to use subarray coherence for the SCBP design and combined it with the MV or ESBMV weight. In fact, if the subarray size L=M, namely no spatial smoothing is used, and with a DAS weighting function, the SCBP of expression (19) will degenerate to the Wiener postfilter for the DAS beamformer with white noise assumption. This builds the relationship between the SCBP and the Wiener postfilter. If the subarray size L=1, which means there is no summation process in the subarray, the SCP should be the same as the SICP and the H_{SCBP} will not be affected. The results from this study showed that the proposed method is valid in enhancing the imaging quality over the DAS, MV and ESBMV beamformers. The imaging resolution enhancement of the ESBMV-SCBP is similar to that of the ESBMV-Wiener beamformer, with better imaging contrast resulting from a better preservation of the speckle pattern. As for the computational complexity, the additional computation amount is relatively small since the coherent or incoherent energy computation is only $O(L^2)$, while the MV or ESBMV weights computation has a complexity of $O(L^3)$ [18, 27].

The proposed ESBMV-SCBP beamformer achieved an improved imaging quality compared to the ESBMV beamformer. However, the problem in choosing the eigenvalue threshold was not totally solved. In plane-wave imaging, the image suffers a low SNR. This makes it hard to use a proper eigenvalue threshold β to reduce the noise inside the cyst perfectly without causing distortion to the speckle. Moreover, as plane-wave imaging usually leads to a high sidelobe, even a small β may severely damage the distortionless constraint in the speckle region alongside high intensity targets and cause black artifacts. One method to improve this is to select the eigen vectors that have the closer direction to the steering vector, since ideally the direction of the steering vector and noise subspace should be orthogonal [18]. In this paper, we suggested to set a small threshold β to preserve the signal parts and the near-distortionless property. The underestimated noise was then suppressed by the proposed ESBMV-SCBP. In practical application, an alternative way to determine the value of β according to the types of the imaging object

should be explored. One approach is to use an SNR analysis scheme to determine the β value adaptively, just similar as that used in [22] to determine the scaled factor η. This SNR dependent scheme for the scaled factor η may also be applied in our SCBP design, to pursue a better imaging quality in future studies.

6. Conclusion

The ESBMV-SCBP beamformer was proposed and validated for ultrasound plane-wave imaging in this study. We analyzed the MV-based beamformers and the CF-based beamformers and pointed out the effect of the spatial smoothing on the postfilter design. The ESBMV-SCBP scheme was then proposed based on the subarray domain and applied to both simulated and experimental plane-wave imaging data. The results showed that the ESBMV-SCBP is effective in improving the imaging quality over the DAS, MV, and ESBMV beamformers. The improvement of the ESBMV-SCBP was also demonstrated to be comparable to that of the ESBMV-Wiener in terms of resolution, and better in terms of contrast and structure visualization. Only a small extra computation cost was needed to achieve this improvement. Thus, the proposed method has potential in enhancing the quality of the ultrasound plane-wave imaging.

Acknowledgements

This work was supported by the National Basic Research Program of China (2015CB755500), the National Natural Science Foundation of China (61271071, 11474071, 81101049), Doctoral Fund of Ministry of Education (20110071 120019), and the Joint Supervision Scheme with Mainland China, Taiwan and Macao University of Hong Kong Polytechnic University (G-SB19). The authors would like to thank Ms Sally Ding for her help in editing the manuscript.

References

[1] D. Garcia, L. Le Tarnec, S. Muth, E. Montagnon, J. Poree, G. Cloutier, Stolt's f-k Migration for Plane Wave Ultrasound Imaging, IEEE Transactions on Ultrasonics Ferroelectrics and Frequency Control, 60 (2013) 1853-1867.

[2] M. Tanter, M. Fink, Ultrafast Imaging in Biomedical Ultrasound, IEEE Transactions on Ultrasonics Ferroelectrics and Frequency Control, 61 (2014) 102-119.

[3] L. Sandrin, M. Tanter, S. Catheline, M. Fink, Shear modulus imaging with 2-D transient elastography, IEEE Transactions on Ultrasonics Ferroelectrics and Frequency Control, 49 (2002) 426-435.

[4] G. Montaldo, M. Tanter, J. Bercoff, N. Benech, M. Fink, Coherent Plane-Wave Compounding for Very High Frame Rate Ultrasonography and Transient Elastography, IEEE Transactions on Ultrasonics Ferroelectrics and Frequency Control, 56 (2009) 489-506.
[5] B. Denarie, T.A. Tangen, I.K. Ekroll, N. Rolim, H. Torp, T. Bjastad, L. Lovstakken, Coherent Plane Wave Compounding for Very High Frame Rate Ultrasonography of Rapidly Moving Targets, IEEE Transactions on Medical Imaging, 32 (2013) 1265-1276.
[6] B.M. Asl, A. Mahloojifar, Minimum Variance Beamforming Combined with Adaptive Coherence Weighting Applied to Medical Ultrasound Imaging, IEEE Transactions on Ultrasonics Ferroelectrics and Frequency Control, 56 (2009) 1923-1931.
[7] B.M. Asl, A. Mahloojifar, Eigenspace-Based Minimum Variance Beamforming Applied to Medical Ultrasound Imaging, IEEE Transactions on Ultrasonics Ferroelectrics and Frequency Control, 57 (2010) 2381-2390.
[8] I.K. Holfort, F. Gran, J.A. Jensen, Broadband Minimum Variance Beamforming for Ultrasound Imaging, IEEE Transactions on Ultrasonics Ferroelectrics and Frequency Control, 56 (2009) 314-325.
[9] J.-F. Synnevag, A. Austeng, S. Holm, Adaptive beamforming applied to medical ultrasound imaging, IEEE Transactions on Ultrasonics Ferroelectrics and Frequency Control, 54 (2007) 1606-1613.
[10] J.-F. Synnevag, A. Austeng, S. Holm, Benefits of Minimum-Variance Beamforming in Medical Ultrasound Imaging, IEEE Transactions on Ultrasonics Ferroelectrics and Frequency Control, 56 (2009) 1868-1879.
[11] A.E.A. Blomberg, C.-I.C. Nilsen, A. Austeng, R.E. Hansen, Adaptive Sonar Imaging Using Aperture Coherence, IEEE Journal of Oceanic Engineering, 38 (2013) 98-108.
[12] P.C. Li, M.L. Li, Adaptive imaging using the generalized coherence factor, IEEE Transactions on Ultrasonics Ferroelectrics and Frequency Control, 50 (2003) 128-141.
[13] J.P. Asen, J.I. Buskenes, C.-I.C. Nilsen, A. Austeng, S. Holm, Implementing Capon Beamforming on a GPU for Real-Time Cardiac Ultrasound Imaging, Ieee Transactions on Ultrasonics Ferroelectrics and Frequency Control, 61 (2014) 76-85.
[14] B.Y.S. Yiu, A.C.H. Yu, GPU-BASED MINIMUM VARIANCE BEAMFORMER FOR SYNTHETIC APERTURE IMAGING OF THE EYE, Ultrasound in Medicine and Biology, 41 (2015) 871-883.
[15] J. Capon, High-resolution frequency-wavenumber spectrum analysis, Proceedings of the IEEE, 57 (1969) 1408-1418.
[16] B.M. Asl, A. Mahloojifar, Contrast Enhancement and Robustness Improvement of Adaptive Ultrasound Imaging Using Forward-Backward Minimum Variance Beamforming, IEEE Transactions on Ultrasonics Ferroelectrics and Frequency Control, 58 (2011) 858-867.
[17] A.C. Jensen, A. Austeng, An Approach to Multibeam Covariance Matrices for Adaptive Beamforming in Ultrasonography, IEEE Transactions on Ultrasonics Ferroelectrics and Frequency Control, 59 (2012) 1139-1148.
[18] S. Mehdizadeh, A. Austeng, T.F. Johansen, S. Holm, Eigenspace Based Minimum Variance Beamforming Applied to Ultrasound Imaging of Acoustically Hard Tissues, IEEE Transactions on Medical Imaging, 31 (2012) 1912-1921.
[19] X. Zeng, C. Chen, Y. Wang, Eigenspace-based minimum variance beamformer combined with Wiener postfilter for medical ultrasound imaging, Ultrasonics, 52 (2012) 996-1004.
[20] C.-I.C. Nilsen, S. Holm, Wiener Beamforming and the Coherence Factor in Ultrasound Imaging, IEEE Transactions on Ultrasonics Ferroelectrics and Frequency Control, 57 (2010) 1329-1346.
[21] S.-L. Wang, P.-C. Li, MVDR-based coherence weighting for high-frame-rate adaptive imaging, IEEE Transactions on Ultrasonics Ferroelectrics and Frequency Control, 56 (2009) 2097-2110.
[22] Y.-H. Wang, P.-C. Li, SNR-Dependent Coherence-Based Adaptive Imaging for High-Frame-Rate Ultrasonic and Photoacoustic Imaging, IEEE Transactions on Ultrasonics Ferroelectrics and Frequency Control, 61 (2014) 1419-1432.
[23] M. Xu, X. Yang, M. Ding, M. Yuchi, Spatio-Temporally Smoothed Coherence Factor for Ultrasound Imaging, IEEE Transactions on Ultrasonics Ferroelectrics and Frequency Control, 61 (2014) 182-190.
[24] B.M. Asl, A. Mahloojifar, A Low-Complexity Adaptive Beamformer for Ultrasound Imaging Using Structured Covariance Matrix, IEEE Transactions on Ultrasonics Ferroelectrics and Frequency Control, 59 (2012) 660-667.
[25] S.M. Sakhaei, Optimum beamforming for sidelobe reduction in ultrasound imaging, IEEE Transactions on Ultrasonics Ferroelectrics and Frequency Control 59 (2012) 799-805.
[26] J.A. Jensen, Field: A program for simulating ultrasound systems, in: 10TH NORDICBALTIC CONFERENCE ON BIOMEDICAL IMAGING, VOL. 4, SUPPLEMENT 1, PART 1: 351--353, Citeseer, 1996.

[27] G.H. Golub, C.F. Van Loan, Matrix computations, JHU Press, 2012.